Observations on bubble shapes in bubble columns under different flow conditions

Ziegenhein, T.; Lucas, D.;

Originally published:

March 2017

Experimental Thermal and Fluid Science 85(2017)1, 248-256

DOI: https://doi.org/10.1016/j.expthermflusci.2017.03.009

Perma-Link to Publication Repository of HZDR:

https://www.hzdr.de/publications/Publ-24384

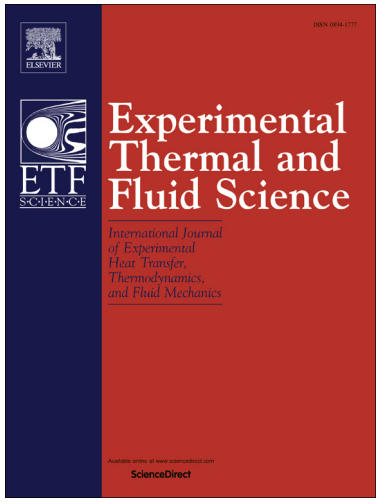

Observations on bubble shapes in bubble columns under different flow conditions

T. Ziegenhein, D. Lucas

PII: S0894-1777(17)30066-3
DOI: http://dx.doi.org/10.1016/j.expthermflusci.2017.03.009
Reference: ETF 9039

To appear in: *Experimental Thermal and Fluid Science*

Received Date: 9 November 2016
Revised Date: 2 March 2017
Accepted Date: 3 March 2017

Please cite this article as: T. Ziegenhein, D. Lucas, Observations on bubble shapes in bubble columns under different flow conditions, *Experimental Thermal and Fluid Science* (2017), doi: http://dx.doi.org/10.1016/j.expthermflusci.2017.03.009

Observations on bubble shapes in bubble columns under different flow conditions

T. Ziegenhein* and D. Lucas

Helmholtz-Zentrum Dresden-Rossendorf e.V., 01314 Dresden, Germany

* Corresponding author. Tel.: +49 3512602503; fax: +49 3512603440.
E-mail address: t.ziegenhein@hzdr.de (Thomas Ziegenhein).

ABSTRACT

The bubble shape is fundamental for every aspect of modelling bubbly flows. The interface is usually highly deformable so that the bubble shape is in general dependent on the surrounding turbulent flow field. Since recent work on this topic addressed almost entirely single-bubbles rising in quiescent flow, the extent of such flow field dependencies as well as swarm effects is rather unknown. This study examines the effect on the bubble shape in bubbly flows with a liquid background flow that is generated by natural convection in the bubbly flow regime when flow properties, i.e. the gas flow rate, sparger setup, and column geometry, are changed by evaluating six different bubble column experiments. The results of this integral approach reveal that the bubble shape of small bubbles is distinctly influenced whereas the shape of large bubbles is unchanged. Averaged over all flow rates, we find that the size-dependent bubble shapes are quite similar for all six experiments. Further studies focusing on single local effects like the shear rate or wake effects are highly desirable to obtain a deeper understanding of the underlying processes; for this purpose, the given results can help to assess the most important effect and in which extend it should be studied.

KEYWORDS

Bubble shape, Bubbly flows, Bubble column, Turbulent flow, Swarm effects

1 Introduction

Knowing the interface size and shape is crucial to characterize multiphase flows properly. The problem gets complicated if the interface interacts with the surrounding flow so that its size and shape depends on the flow properties. Especially for ellipsoid bubbles at medium to high Eötvös numbers and low Morton numbers, the modelling effort becomes vast in turbulent flows, which determine the interface size predominantly. In low turbulence, however, the problem is appropriately simplified by assuming rotationally symmetric ellipsoids defined solely by the major and minor axis. In such flows, the aspect ratio, besides of the bubble size, is only needed to describe the shape.

The significance of the bubble shape is made clear by studying the way separate effects of bubbly flows are modeled. Drag force models have to contain the information about the bubble shape, which is, indeed, inherently included (Grace et al. 1976). Seldom are the deformation and the surface friction separately modeled, as for example Bozzano & Dente (2001) proposed. Another very important effect is the shear induced lift force on bubbles, which seems to be directly influenced by the major axis (Tomiyama et al. 2002). Further, the interface size and shape characterize the heat and mass exchange in bubbly flows. Briefly speaking, the aspect ratio is a basic parameter for modeling and understanding bubbly flows.

The common strategy in bubbly flows is to study effects at single bubbles and apply the obtained models to complex flows. This was also done extensively for the aspect ratio over the past few decades. Loth (2008) provides an extensive review to this topic and Liu et al. (2015) give a detailed literature overview to bubble shape models in quiescent flow so that this is not repeated at this point. Despite its importance, a comprehensive evaluation of the aspect ratio under realistic flow conditions is not yet published. It is therefore necessary to study the extent to which the surrounding flow affects the bubble shape.

To confine this enormous task, the bubble shape in low turbulence flow, which is found in bubbly flows without external driving force, at low to medium void fractions, will be studied in this work. In doing so, six bubble column experiments, which range from single bubbles in moderate shear flows to airlift reactors, are evaluated at different flow conditions. Simplifying it even further, only integral dependencies are studied; in particular by changing the gas flow rate, the column geometry and the sparger setup. A local evaluation of the bubble shape considering for example the liquid velocity gradients or turbulence levels is highly desirable but requires an enormous database as well as measuring all quantities at the same time. Such detailed studies are little published in literature or not possible now for appropriate void fractions so that an integral evaluation is justified at this point. By means of the Morton, Eötvös and Reynolds number, which are defined by Equation (1), the aspect ratio will be compared to literature data obtained with single bubbles in quiescent flow and the bubble column data from Besagni & Inzoli (2016); further, the distribution of the aspect ratio will give a deeper understanding of the different observations.

$$Eo = \frac{\Delta\rho g d_B^2}{\sigma}, Re = \frac{\rho v_{rel} d_B}{\mu}, Mo = \frac{g\mu^4\Delta\rho}{\rho^2\sigma^3} \quad (1)$$

For this purpose, the bubble size, d_B, is defined as the spherical equivalent diameter of the rotational volume of the projected bubble area recorded by a high-speed camera, the major axis is defined as the longest distance between two points of the projected bubble area, and the minor axis is the longest distance perpendicular to the major axis. This procedure is demonstrated in Figure 1 with a measured bubble boundary. The definition of the major and minor axes, however, is not always obvious, e.g. Bozzano & Dente (2001) constrain the axes to intersect with the bubble center; or, in simulations the surrounding box perpendicular to the gravity is often used (Dijkhuizen et al. 2010). For bubbles that experience significant deformation due to the flow field, we found that the present formulation is suitable since neither the center of the projected bubble area is necessarily related to the axes nor the bubbles are aligned with gravity.

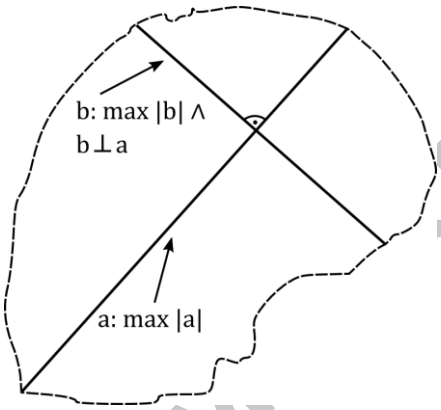

Figure 1 Definition of the major axis, which is marked as 'a' in the graph, and the minor axis, which is marked as 'b'.

2 Experimental setups

To serve the present purpose, experiments at different flow conditions have to be considered. From our own experimental database, we had chosen four typical bubble column experiments, one experiment dealing with single bubbles in different shear flows, and different experiments with a single needle-sparger. All experiments were conducted in purified water and filtered air; the water was replaced every 4 to 8 hours.

The experiments are summarized in Table 1. Here, the inner diameter of the used needles in the sparger (vertical) are shown with the corresponding flow rates. Nonetheless the inner needle diameter is not explicitly studied in the present work, it is the naturally way the experiments were organized so that it gives an insight how the data were obtained. In addition, the range of bubble sizes and the shape regimes that are covered in the present work are sketched in Figure 2. The four bubble column experiments studied consist of two bubble plume experiments ("BP1" and "BP2" in Table 1), which have an interval of two years in between, an airlift reactor ("AL"), which is also described previously by Ziegenhein, et al. (2016), and a homogenously aerated bubble column ("Hom"). The gas sparger can hold up to twelve needles; different needle sizes operated at different flow rates produce the desired variety of bubble sizes. For some experiments, plastic "caps" on the needles were used to generate large bubbles at very low flow rates. In these caps, the bubbles are decelerated so that they can coalescence before they leave.

Table 1 Experimental matrix, flow rates through the complete sparger (horizontal) versus the inner diameter of the used needles is shown. Abbreviations: Bubble plume 1 (BP1), bubble plume 2 (BP2), homogenously aerated bubble column (Hom), air lift reactor (AL)

l/min / mm	0	0 - 0.7	0.6	1	1.8	2.4	3	4	4.5	4.8	6
0.12	Single bubble in shear flow	Single needle		Hom							
0.2			BP1		BP1	Hom	BP1				
0.3				Hom	BP1					BP1	
0.5											
0.6				Hom			AL | BP2	BP2	AL		AL
0.7			BP1				BP1			BP1	BP1
0.9				Hom							
1.5					BP1	Hom	BP1|BP2	BP2		BP1	BP1
Caps				Hom							
1.5/0.6							BP2			BP2	

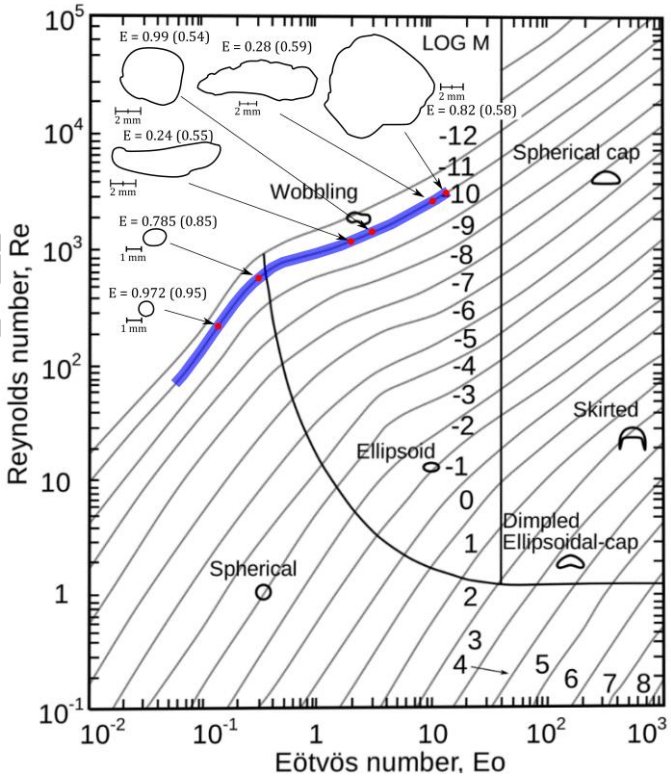

Figure 2 Grace Diagram (Grace et al. 1976) with the size range highlighted that is investigated in the present work. Selected shapes of bubbles are shown with the aspect ratio, E, of the bubble and the averaged aspect ratio of the size class in brackets.

The dimensions of the used bubble columns are shown in Figure 3. The downcomer's width (*W*) of the airlift reactor is here constant with 0.06 m; the sparger size (*S*) varies from 0.085 m to 0.035 m. The height (*H*) of the bubble plume experiments and the single needle experiment ranges from 0.7 to 0.9 m; the sparger size varies from 0.085 m to 0.035 m. The not shown single needle experiment was conducted in the bubble plume setup but with only one sparger needle in the center.

The not shown single bubble experiment in different shear flows is similar to the bubble plume setup; single bubbles were generated at the left side whereas at the right wall many large bubbles rise generating a vortex in which the areas with a linear shear field were evaluated for the present study. The produced shear rates were in the range of 2 s^{-1} to 3 s^{-1}; the turbulent kinetic energy was relatively low in the range from 0.000875 $\mathrm{m}^2/\mathrm{s}^2$ to 0.00175 $\mathrm{m}^2/\mathrm{s}^2$. For these experiments, the liquid velocity was measured with PIV as described by Ziegenhein & Lucas (2016); the liquid velocity was separately measured to not contaminate the bubbles with the PIV tracer particles. For the single needle experiments, the liquid velocity was not measured. All experiments were conducted in bubble columns operating in batch mode so that the liquid velocity field was completely determined by the recirculation induced by buoyancy.

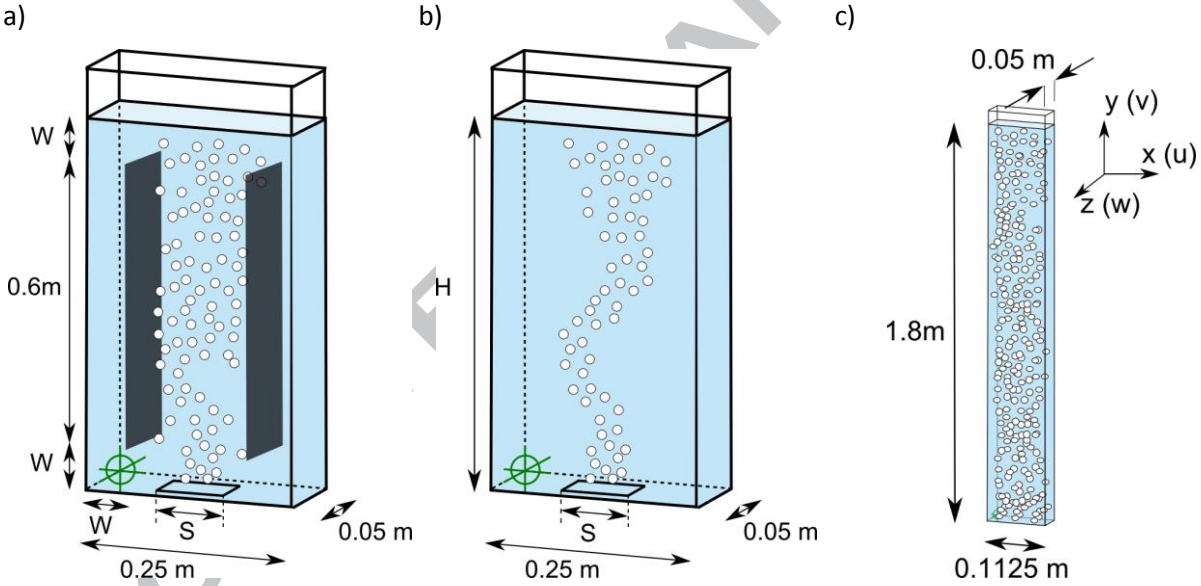

Figure 3 Experimental setup of the airlift a), bubble plume 1 and 2 as well as single needle experiments b), and the homogenously aerated bubble column c)

Except of the homogenously aerated bubble column, the liquid velocity field of the other experiments was determined with particle tracking using natural micro bubbles (Ziegenhein et al. 2016) to not contaminate the flow with tracer particles. In the homogenously aerated column, no natural micro bubbles occurred so that the flow was seeded with 100 µm PMMA particles. Exemplary, the vertical liquid velocities v as well as the normal Reynolds stress tensor component $v'v'$ at $y = 0.6$ m for the riser of the airlift, bubble plume 1, and the homogenously aerated column are shown in Figure 4. Typically, the velocity profile measured in the homogenously aerated column is flat whereas in the airlift and bubble plume the profile is center peaked. Likewise, the $v'v'$ profile in the homogenously aerated column is the lowest. The peak beside the center in the $v'v'$ profile of the bubble plume is typical for

such setups. The same can be observed in the airlift reactor's riser since the circulating flow confines the bubbles generated at the bottom so that a bubble plume occurs, which is spreading fast towards the top. Summarizing, from our experience the shown velocity fields represent the typical measured values in such bubble columns.

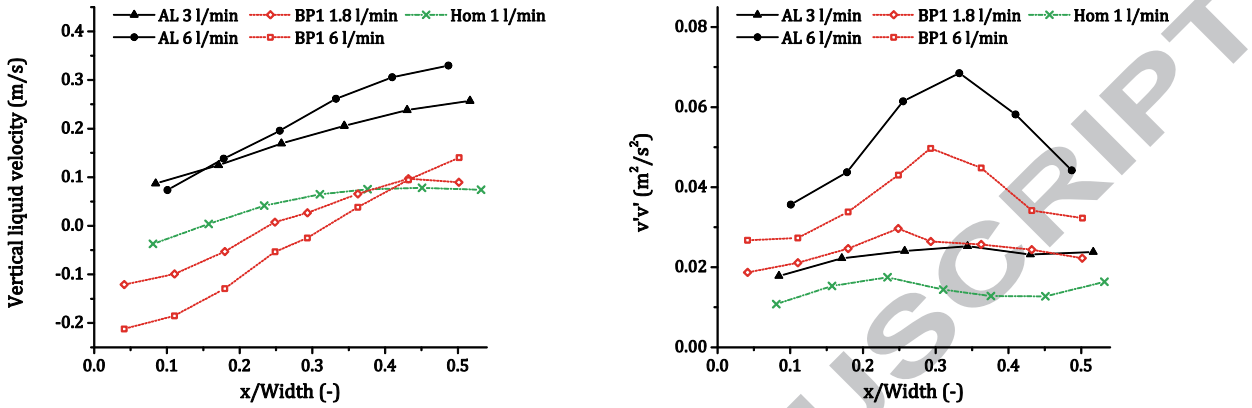

Figure 4 Measured vertical liquid velocity (v) and the normal Reynolds stress tensor component $v'v'$ for different setups (see Table 1 for abbreviations) and flow rates at $y = 0.6\,m$. For the airlift reactor, only the results in the riser are shown. Due to symmetry, only one-half of the column is shown.

For all experiments, purified water was used. To assess the water quality by a quantitative value, the slip velocity might be reasonable to use (Figure 5). The results from the single bubble experiments in shear flows are situated between the model of Tomiyama et al. (1998) for pure conditions and the model of Bozzano & Dente (2001) so that it can be safely assumed that the water used is sufficiently clean. In an interval of one year, this experiment was repeated, with the same result. Hence, for all experiments in the present study, which were realized within three years, the water quality might be the same.

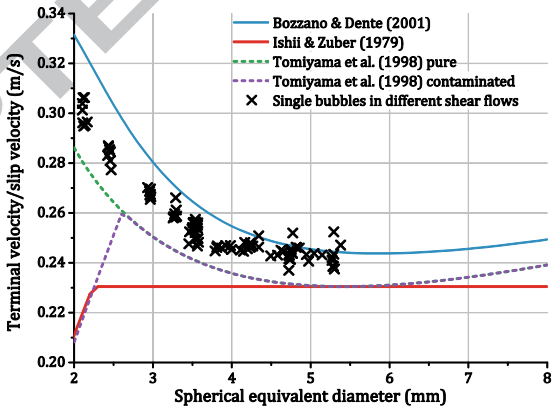

Figure 5 Measured slip velocity compared to different terminal velocity models

As mentioned above, the projected bubble size area was used to calculate the major and minor axes as well as the bubble size, which is here the spherical equivalent diameter of the rotational volume of the projected area of single photographs. For the single bubble experiments the photographs were evaluated automatically and for all other experiments by hand with support of automated image analyzes. Both techniques are described in our previous work (Ziegenhein et al. 2016). The error of extracting the projected area is negligible due to a very high image resolution of 50 - 250 µm/Pixel and

the by hand evaluation of the images. Representative pictures that were used for the bubble size evaluation are shown in Figure 6.

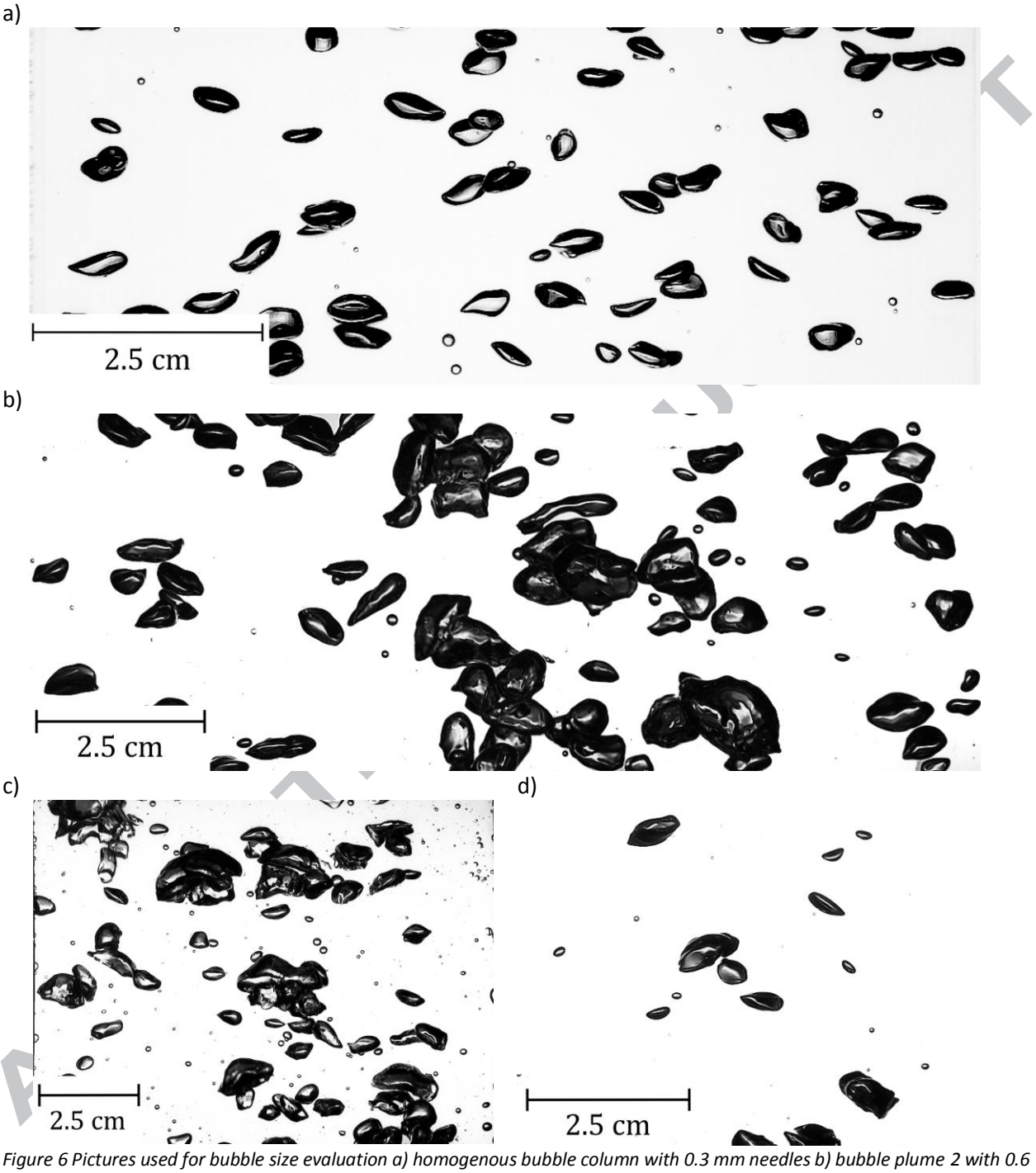

Figure 6 Pictures used for bubble size evaluation a) homogenous bubble column with 0.3 mm needles b) bubble plume 2 with 0.6 mm needles and a gas flow rate of 4.0 l/min c) airlift reactor at a gas flow rate of 4.5 l/min and d) single needle experiment with 0.6 mm needles and 0.5 l/min.

The assumption of a rotational ellipsoid is valid in single bubble experiments (Liu et al. 2015), what we can confirm for our single bubble experiments in shear flows. In the bubble column experiments the three dimensional shape is not accessible with photographic techniques so that the following results are

confined to the projected area. The bubble sizes were evaluated at different levels in the bubble columns, which were all sufficiently away from the sparger. Since we did not found any height dependency of the bubble shape, the results of the different levels were summed up for the single experiments. Following the integral approach of the present work, we evaluated the bubbles always over the complete flow cross section. Since the method for evaluating the bubble size in swarms used (Ziegenhein et al. 2016) needs several pictures, we recorded 10 pictures with around 200 fps with a pause of one second between the bursts; usually, 100 bursts were recorded. This procedure was repeated three times with around 5 minutes in between; the pictures used for evaluation were chosen arbitrarily from this set. The count of tracked bubbles was determined by demanding a converging bubble size distribution; usually 1000 to 4000 bubbles were tracked per measurement, depending on the width of the bubble size distribution. The count of the tracked bubbles and the standard error of the major axis, which we found is usually two orders of magnitude larger than the standard error of the bubble size, are shown in Figure 7.

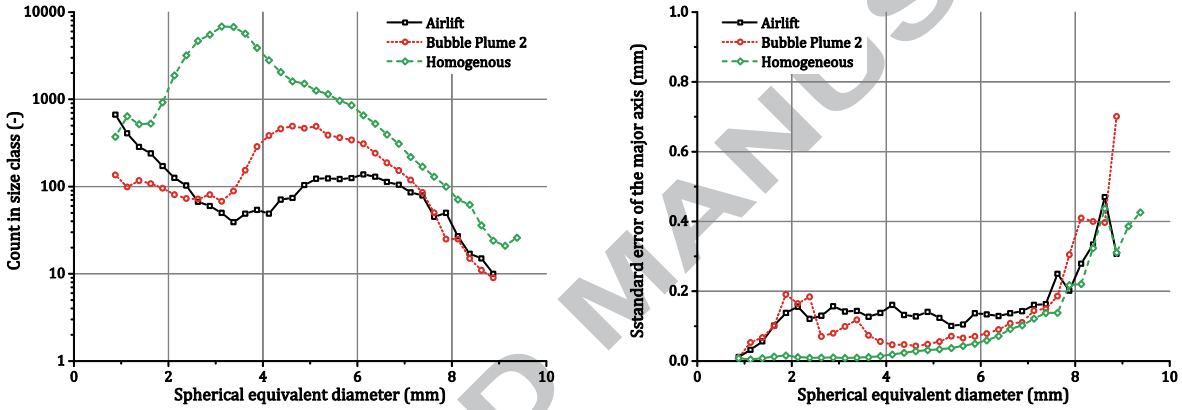

Figure 7 The bubble count (left) and the standard error $\left(=\frac{1}{\sqrt{N}}\sigma\right)$ *of the major axis (right) for the Airlift, Bubble Plume 2, and Homogenous experiment with respect of 0.25 mm bubble size classes.*

The bubble size distributions are very different for the cases considered (Figure 8). At low gas flow rates and for the homogenous cases, the distributions are narrow without very large bubbles; at higher flow rates, on the other hand, the distributions are wide with very large bubbles. Besides the higher gas void fraction at higher flow rates, the flow was much more disturbed because of the wide range of bubble sizes so that in general much more bubble-bubble interactions were observed for these cases. However, these two effects, higher void fraction and wider bubble size distribution, are separated for the airlift reactor cases. Here, we obtained almost exactly the same bubble size distributions by keeping the flow rate per needle constant for all cases but increasing the void fraction by enlarging the gas sparger (Ziegenhein et al. 2016).

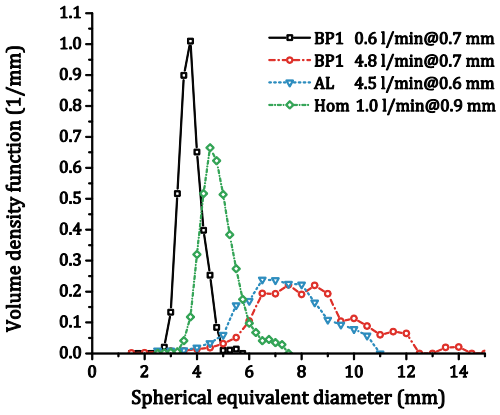

Figure 8 Bubble size distribution for different gas flow rates and needle sizes.

3 Results and discussion

3.1 Different gas flow rates

In bubble columns, the gas flow rate determines the local gas volume fraction that determines, on the other hand, all flow parameters. Consequently, studying the aspect ratio E at different flow rates gives an idea if and in which extent the bubble shape is affected when the flow conditions are changed. Nevertheless, with this approach it cannot be determined in which extend local flow values like the shear rate influence the bubble shape. In the worst case, it is possible that different effects are compensated by just increasing the flow rate.

The general trend of almost spherical small bubbles and ellipsoidal large bubbles is observed for all flow rates. In the riser of the airlift reactor (Figure 9), changing the flow rate, however, does not influence the bubble shape significantly overall. Considering the flow field (Figure 4), the circulating liquid dominates the flow in the airlift reactor; even at a gas flow rate of 3 l/min, the liquid velocity is relatively high. The $v'v'$ values, on the other hand, are distinctly different. The void fraction, which ranges from around 3.5% for 3.0 l/min to 7% for 6.0 l/min, seems to not influencing the bubble shape as well.

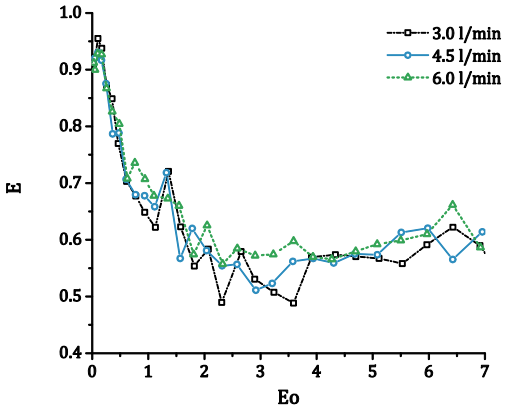

Figure 9 Aspect ratio at different gas flow rates in the riser of the airlift reactor.

The bubble plume 1 experiment (Figure 10) gives a different picture; for small bubbles, the aspect ratios increase with higher flow rates, whereas they approach each other for larger bubble sizes. Comparing the flow field of the bubble plume with the airlift reactor in Figure 4, the distinct backflow at the walls with a slightly steeper averaged velocity profile is the most obvious difference, whereas, the $v'v'$ profiles are similar. The $v'v'$ profiles in the bubble plume experiment, however, originate predominantly from the large-scale transient swinging motion of the bubble plume, especially at low gas flow rates. In addition, the bubble size distribution in the bubble plume experiment is changing with the flow rates in contrast to a constant bubble size distribution in the airlift reactor for all flow rates (Figure 8). Since the bubble shape is not changing with higher flow rates in the airlift reactor, it might be concluded that the bubble shape depends rather on the bubble size distribution and present flow regime than the void fraction for this case. However, due to the larger bubbles in a wide bubble size distribution, the bubbly flow can be considered as "instable" (Lucas et al. 2005) in general so that higher local velocity gradients, possible more bubble-bubble interactions, and higher turbulence can be expected.

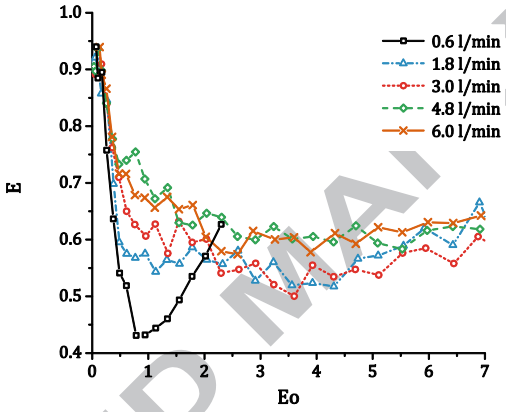

Figure 10 Aspect ratios for the bubble plume experiment BP1 at different gas flow rates.

The biggest difference between the single gas flow rates is observed around $\mathrm{Eo} = 1$. This difference can be well studied by means of the number density distribution of the aspect ratio between $0.75 \leq \mathrm{Eo} \leq 1.25$ (Figure 11). At the lowest flow rate, the distribution is narrow with a distinct peak at around $\mathrm{E} = 0.45$. At higher flow rates, on the other hand, the distributions are considerably wider, shifted to higher aspect ratios, and without a clear peak. Noticeable are the almost spherical bubbles found at 4.8 l/min and above. We observed that the flow distinctly deforms the bubbles so that the shape oscillations ("wobbling") are different from lower flow rates; here, the bubbles appeared sometimes spherical.

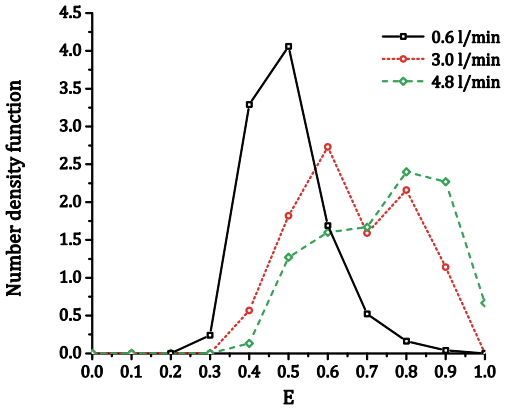

Figure 11 Number density distribution of the aspect ratio in the range $0.75 \leq Eo \leq 1.25$

3.2 Different experimental setups

Besides the influence of the gas flow rate, also the experimental setup determines the flow conditions inside bubble columns. In the homogenously aerated column, large-scale fluctuations are not dominant, whereas such dominate the bubble plume experiments. Inside the riser of airlift reactors, a distinct background flow is observed so that large scales (bubble plume) and small scales are present. The different single-phase background flows, on the other hand, completely determine the single bubble experiments. The single needle experiments can be interpreted as bubble plumes at very low gas flow rates; the bubbles do not ascent in a steady state but might be still less influenced by the background flow.

Comparing the aspect ratios of the different experiments, which are averaged over all gas flow rates and needle setups, relatively small but distinct differences can be observed (Figure 12). The single needle and single bubble experiments exhibit the smallest aspect ratios and are almost on top of each other. The aspect ratios observed in the airlift reactor show that the bubbles are, largely, the least oblate in this setup. Again, distinct differences are observed at smaller bubbles, whereas the aspect ratios approach each other with increasing bubble size; above $\mathrm{Eo} = 8$ all experiments are almost on top of each other.

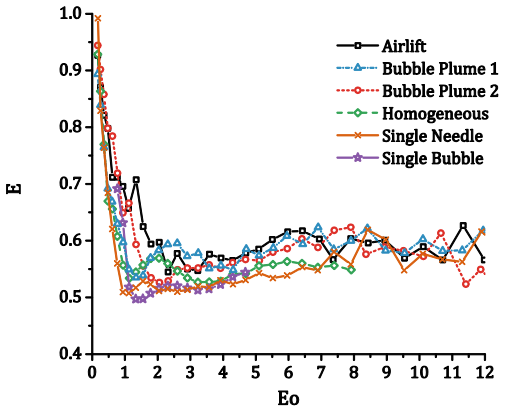

Figure 12 Aspect ratios for different experiments.

Referring to the number density distribution of the aspect ratios at smaller bubble sizes in Figure 13, the differences between the experiments can be seen nicely. The distribution obtained in the airlift reactor is distinctly wider compared to the others. Surprisingly, the single bubble distribution and the distribution obtained in the bubble plume 1 experiments as well as the homogenously aerated column have almost the identic shape; solely, the single bubble distribution is a little bit shifted towards smaller aspect ratios.

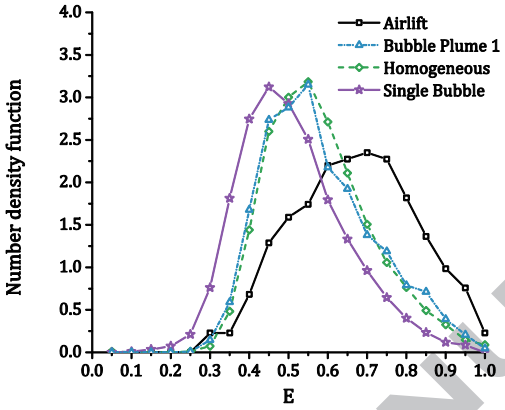

Figure 13 The aspect ratio distribution in the range $1 < Eo < 2$

A completely different situation can be observed at larger bubble sizes (Figure 14); the distributions are almost equal in shape and position. Again, a small shift of the single bubble experiments to smaller aspect ratios can be observed. In conclusion, not only the averaged aspect ratios approach each other at larger bubble sizes but also their distributions.

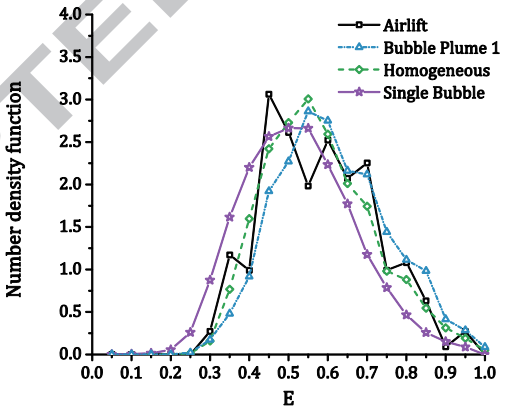

Figure 14 The aspect ratio distribution in the range $2 < Eo < 3$

Different aspect ratios are observed in the different experimental setups. The single needle experiment and the single bubble experiment with background flow, however, are almost equal. Interestingly, the aspect ratios measured in the homogenously aerated bubble column are comparable to the aspect ratios observed in these two experiments. In addition, the reproducibility of the experiments is indicated by the almost equal ratios obtained for the two different bubble plume experiments. As would be expected, the aspect ratios observed in the airlift reactor, in which the highest turbulence was

measured, are mostly the highest. The aspect ratio distributions reveal that larger bubbles have almost the same shape in all experiments.

3.3 Comparison with literature

Detailed studies about the bubble shape from steady state rising single bubbles in quiescent flow can be found in the literature. To compare the results from the present study with these studies, the aspect ratios obtained from the single experimental setups are averaged. More precisely, the single bubble experiments with background flow for which over one million bubbles were tracked contribute to the averaged values in the same way as the airlift experiments with around twenty thousand bubbles measured.

Referring to the Eötvös number, the results are compared with the well-known correlation of Wellek et al. (1966), the correlation for super-purified water measured by Sanada et al. (2008), the fit of Besagni & Inzoli (2016) to their experimental data obtained in an annular gap bubble column ($Eo < 11$), and the fit of Liu et al. (2015) to their single bubble experiments in Figure 15. Interestingly, small bubbles observed in the present experiments with $Eo < 1$ have an aspect ratio similar to those observed in the super-purified water experiments. The aspect ratios for larger bubbles are more or less constant with respect to the different experimental setups; and are in good agreement with the fit to the monotonously decreasing Wellek formulation of Liu et al. and Besagni & Inzoli. In quiescent flow, however, several studies report an influence of the initial bubble formation on the shape (e.g. by Liu, et al. (2015)). Certainly, the Eötvös number cannot cover this effect so that the Weber number, which includes the influence of the slip velocity, might be a more appropriate dimensionless number (Okawa et al. 2003).

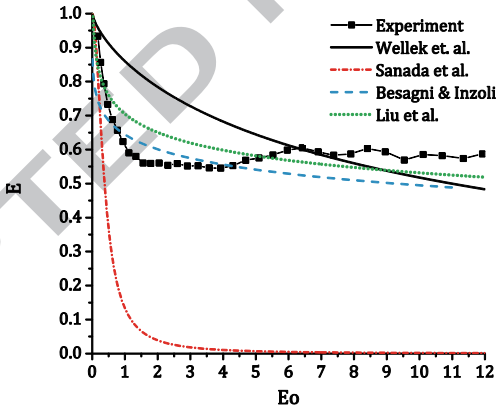

Figure 15 Aspect ratios as a function of the Eötvös number.

In complex bubbly flows, however, the slip velocity is not known and hardly measureable; using an explicit formula for the slip velocity to estimate the bubble shape in such flows is not meaningful since the shape determines the slip velocity. Nevertheless, as a first assumption the terminal velocity determined from single bubble experiments can be used to assess the Weber number.

For this purpose, the model for the drag coefficient by Tomiyama et al. (1998) in clean conditions (cf. Figure 5) as well as the model by Ishii & Zuber (1979), for comparison, is used. The differences between these two models are, obviously, only for small bubbles present. Both results, however, are again not covered by the literature data over the complete range of Weber numbers (Figure 16). For large Weber

numbers, the fit of Liu et al. (2015) shows a good conformity with the present results. The correlations of Wellek et al. (1966) and Taylor & Acrivos (1964), on the other hand, cannot reflect the observed aspect ratios.

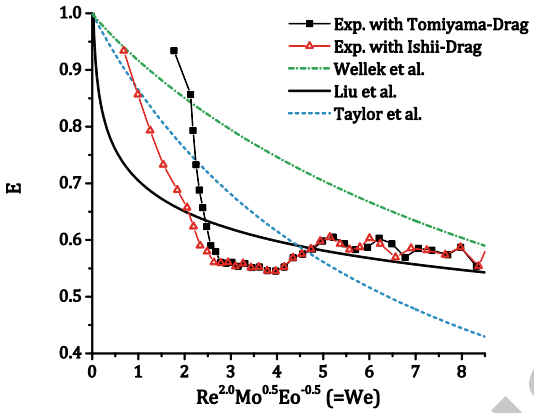

Figure 16 Aspect ratios as a function of the Weber number.

Another way to combine the bubble Reynolds and Eötvös number is called the Tadaki number (Tadaki & Maeda 1961). The observed aspect ratios of the small bubbles fit very well to the correlation by Fan & Tsuchiya (1990) (Figure 17). For larger bubbles, however, the constant aspect ratios with increasing Ta numbers start at $\mathrm{Ta} \approx 3$, which is distinctly smaller as proposed by Fan & Tsuchiya ($\mathrm{Ta} > 20$) as well as proposed by Tadaki & Maeda ($\mathrm{Ta} > 16.5$). In addition, the value of the constant aspect ratios is too high with $\mathrm{E} \approx 0.6$ compared to $\mathrm{E} \approx 0.3$ and $\mathrm{E} \approx 0.23$ proposed by Fan & Tsuchiya and Tadaki & Maeda, respectively. It should be noted that by interpreting the dimensionless numbers as ratios of specific forces, Aoyama et al. (2016) propsed a general form of the Tadaki number for which the contribution of each force can be adjusted. Such an approach might be also usable to evaluate aspect ratios in different flow conditions.

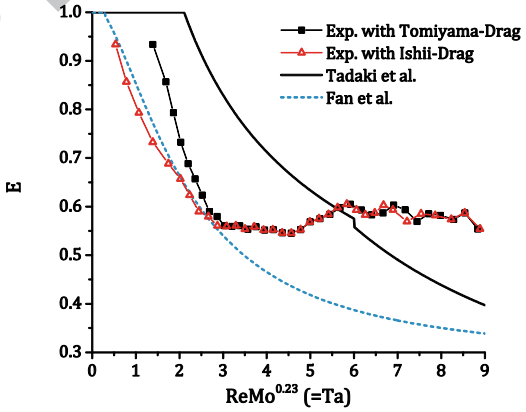

Figure 17 Aspect ratios as a function of the Tadaki number.

Two characteristic behaviors of the observed aspect ratios became obvious; for relatively small bubbles, the aspect ratios decrease and at larger bubble sizes, they stay constant. Every correlation found in the literature describes more or less this behavior, whereas the constant value, in contrast to the present

experiments, is approached asymptotically. The decreasing aspect ratios seem to follow the literature data for super purified water (Sanada et al. 2008) regarding the Eötvös number in good approximation and follow very well the correlation of Fan & Tsuchiya (1990) for purified water regarding the Tadaki number. The determined constant value from the experiments is in the range of the Wellek et al. (1966) correlation, which was originally proposed for drops that might be interpreted as fully contaminated bubbles. The correlation by Liu et al. (2015), however, describes the shape of the large bubbles well.

4 Conclusion

The flow conditions that are present in bubble columns influence the bubble shape. The extent of this effect, however, depends on the bubble size as well as on the flow field. From the results shown in this study, the flow has greater impact on small bubbles than on large bubbles. At larger bubble sizes, the aspect ratios approach each other in all experiments so that it can be concluded that the flow dependency decreases with increasing bubble size and vanish at a certain size. This observation is corroborated by the very good agreement with the bubble shapes found by Besagni & Inzoli 2016 (2016) in an annular gap bubble column and by Liu et al. (2015) in quiescent flow for this size range. This conclusion leaves room for manifold interpretations, from wakes of large bubbles, in which small bubbles are far more often present than other large bubbles, to turbulence length scales, which, when small enough, only affect small bubbles.

In addition, rather the bubble size distribution and the connected local flow field than the hold-up or the averaged turbulent kinetic energy seem to influence the bubble shape. In the shown airlift experiment, the bubble size distribution was kept constant whereas hold-up and turbulent kinetic energy are distinctly changing with higher gas flow rates, the bubble shape, however, was equal for all flow rates. Moreover, when every single experiment is averaged over all flow rates, all experiments show similar bubble shapes. In conclusion, the dependencies of the flow field on the bubble shape should be rather searched local than integral; further, the study of integral parameters like the gas flow rate in the present work can only provide limited access to the underlying processes. In future studies, specially designed experiments that focus only at one parameter are needed. More advanced parameters than the time averaged velocity or void fraction profiles, which may give only a hint on the deeper dependencies, should be considered here.

Nevertheless, some important conclusion regarding modeling of bubbly flows can be drawn from the present study. Regarding CFD simulations, the flow conditions rather less influence the bubble shape in bubble columns compared to other modeling drawbacks (Lucas et al. 2016). The implication is that the bubble shape evaluated at simple flow conditions is very similar to the shape in complex flow conditions, which may be not optical assessable. This makes it very easy to determine bubble shapes in experiments that will be used for CFD validation. In general, the bubble shape should be considered as an input parameter for CFD simulations since the results from single bubble experiments found in the literature cannot represent the shapes from the experiments discussed over the complete size range. In this context, it is moreover reasonable to treat the bubble shape locally and temporal constant in bubble columns as a first assumption. This assumption might be extended to other applications like bubble size measurements via dual tip probes. Nevertheless, in cases in which bubbles have a very long residence time in a column, they might be contaminated even in purified water since impurities accumulate at the interface over time.

Bibliography

Aoyama, S., Hayashi, K., Hosokawa, S. & Tomiyama, A., 2016. Shapes of ellipsoidal bubbles in infinite stagnant liquids. *International Journal of Multiphase Flow,* Volume 79, pp. 23-30.

Besagni, G. & Inzoli, F., 2016. Bubble size distributions and shapes in annular gap bubble column. *Exp Therm Fluid Sci,* Volume 74, pp. 27-48.

Bozzano, G. & Dente, M., 2001. Shape and terminal velocity of single bubble motion: a novel approach. *Computers and Chemical Engineering,* Volume 25, p. 571–576.

Dijkhuizen, W., van Sint Annaland, M. & Kuipers, J. A., 2010. Numerical and experimental investigation of the lift force on single bubbles. *Chemical Engineering Science,* Volume 65, p. 1274–1287.

Fan, L. S. & Tsuchiya, K., 1990. *Bubble Wake Dynamics in Liquids and Liquid–Solid Suspensions.* Oxford: Butterworth-Heinemann.

Grace, J. R., Wairegi, T. & Nguyen, T. H., 1976. Shapes and Velocities of Single Drops and Bubbles Moving Freely Through Immiscible Liquids. *Transactions of the Institute of the Chemical Engineers,* Volume 54, p. 167.

Ishii, M. & Zuber, N., 1979. Drag Coefficient and Relative Velocity in Bubbly, Droplet or Particulate Flows. *AlChE Journal,* Volume 25, p. 843.

Liu, L., Yan, H. & Zhao, G., 2015. Experimental studies on the terminal velocity of air bubbles in water and glycerol aqueous solution. *Exp. Therm. Fluid Sci.,* Volume 62, pp. 109-121.

Loth, E., 2008. Quasi-steady shape and drag of deformable bubbles and drops. *Int. J. Multi. Flow,* Volume 34, pp. 523-546.

Lucas, D., Prasser, H.-M. & Manera, A., 2005. Influence of the lift force on the stability of a bubble column. *Chemical Engineering Science,* Volume 60, p. 3609 – 3619.

Lucas, D. et al., 2016. safety, A strategy for the qualification of multi-fluid approaches for nuclear reactor. *Nuclear Engineering and Design,* Issue 299, pp. 2-11.

Okawa, T., Tanaka, T., Kataoka, I. & Mori, M., 2003. Temperature effect on single bubble rise characteristics in stagnant distilled water. *International Journal of Heat and Mass Transfer ,* 46(5), pp. 903-913.

Sanada, T., Sugihara, K., Shirota, M. & Watanabe, M., 2008. Motion and drag of a single bubble in super-purified water. *Fluid Dynamics Research,* Volume 40, pp. 524-545.

Tadaki, T. & Maeda, S., 1961. On the shape and velocity of single air bubbles rising in various liquids. *Kagaku Kogaku,* Volume 24, pp. 254-264.

Taylor, T. D. & Acrivos, A., 1964. On the deformation and drag of a falling viscous drop at low Reynolds number. *J. Fluid Mech.,* 18(30), pp. 466-476.

Tomiyama, A., Kataoka, I., Zun, I. & Sakaguchi, T., 1998. Drag Coefficients of single bubbles under normal and micro gravity conditions. *JSME International Journal Series B ,* 41(2), p. 472.

Tomiyama, A., Tamai, H., Zun, I. & Hosokawa, S., 2002. Transverse migration of single bubbles in simple shear flows. *Chemical Engineering Science ,* 57(11), pp. 1849-1858.

Wellek, R. M., Agrawal, A. K. & Skelland, A. H. P., 1966. Shape of Liquid Drops Moving in Liquid Media. *AlChE Journal,* Volume 12, p. 854.

Ziegenhein, T., Garcon, M. & Lucas, D., 2016. Particle tracking using micro bubbles in bubbly flows. *Chem. Eng. Sci.,* Volume 153, pp. 155-164.

Ziegenhein, T. & Lucas, D., 2016. On sampling bias in multiphase flows: Particle image velocimetry in bubbly flows. *Flow. Meas. Instrum.,* Volume 48, pp. 36-41.

Ziegenhein, T., Zalucky, J., Rzehak, R. & Lucas, D., 2016. On the hydrodynamics of airlift reactors, Part I: Experiments. *Chem. Eng. Sci.,* Volume 150, pp. 54-65.

- Highlights
  Bubble shape measurements in realistic flow conditions
- Bubble plumes, homogenous bubble columns, airlift reactors, and single bubbles in shear flows are investigated
- Water quality held constant for all experiments
- Flow field for almost all experiments determined